Electronic Supplementary Information: Characterization of Water Dissociation on α-$Al_2O_3(1\bar{1}02)$: Theory and Experiment

Jonas Wirth[a], Harald Kirsch[b], Sebastian Wlosczyk[b], Yujin Tong[b], Peter Saalfrank[a], R. Kramer Campen[b]

[a] *Institute of Chemistry, Karl-Liebknecht Straße 24-25, D-14476, Potsdam, Germany*

[b] *Fritz Haber Institute of the Max Planck Society, Faradayweg 4-6, 14195 Berlin, Germany*

1 Experimental Details

1.1 Sample Preparation and Characterization

For sample mounting we followed previous authors and created a *sandwich* of two α-$Al_2O_3(1\bar{1}02)$ crystals around 0.01 mm thick Tantalum foil secured by Tantalum clips [1]. This mounting allows straightforward control of sample temperature by a combination of liquid N_2 cooling and resistance heating between 130 and 1200 K. The α-$Al_2O_3(1\bar{1}02)$ crystals interrogated in this arrangement were 10 x 15 x 0.5 mm^3 and polished on one side to a roughness < 0.5 nm (as purchased from Princeton Scientific Corp).

Before mounting the sample in the UHV chamber we placed it for 30 minutes in an ultrasonic bath with methanol, dried it with N_2 and rinsed it with milli-pure water for 30 minutes. Mounting this sample in the UHV chamber with no further preparation produces a surface that still shows carbon contamination in Auger Electron spectroscopy (AES). To remove the carbon, we sputtered the sample with 1.5 KV and 3 x 10^{-5}mbar Argon for 30 minutes at multiple spots. As sputtering at such voltages has been shown to produce oxygen vacancies on alumina surfaces [2], we next annealed the sample at 1040 K for 30 minutes in an atmosphere of 5 x 10^{-6} mbar of Oxygen. As shown in Figure 1, this treatment leads to a sample that, when subsequently analyzed with low energy electron diffraction (LEED), produces a sharp (1×1) diffraction pattern and shows no carbon contamination in an AES measurement.

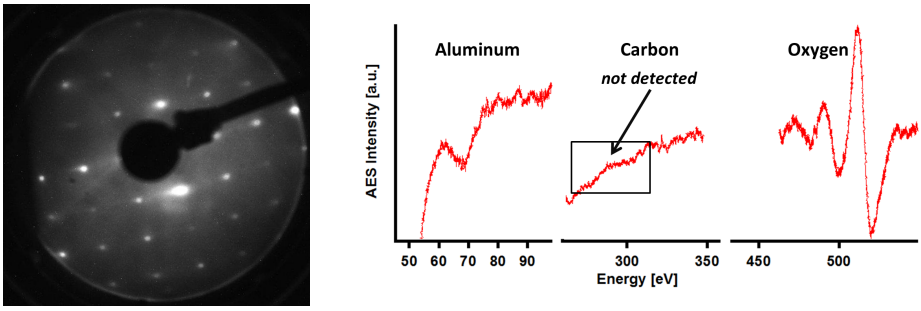

Figure 1: right: (1x1)-LEED pattern and left: Auger spectra of a sputtered and annealed α-$Al_2O_3(1\bar{1}02)$ crystal; LEED pattern is taken at 120 eV

This method of sample preparation was adopted from previous work of Trainor et. al [3], who also generated a surface that gave a well defined (1x1) LEED pattern. Prior work has shown that sputtering and annealing at high temperatures in the *absence* of oxygen will produce a surface with a regular (2×1) LEED pattern [4] that is stable during the subsequent adsorption of water. Given that high energy Ar-ion sputtering is known to create oxygen vacancies on α-Al_2O_3 surfaces [2], we conclude that the high temperature treatment in the absence of oxygen creates a nonstoichiometric surface termination that is oxygen deficient and is not the thermodynamically stable surface termination at moderate temperatures in UHV.

1.2 Temperature Measurement and Control

To measure the sample temperature ($T_{Al_2O_3}$), Chromel/Alumel thermocouples were attached to the crystal edges with ceramic glue (Cerabond 605) and connected to a temperature controller (Model 340, Lakeshore). The temperature controller was also connected to the resistance heating unit. By attaching thermocouples on opposite sides of the crystal, we verified that the sample was heated homogeneously (temperature differences in the plane of the sample surface were < 5 K).

1.3 Water dosing on α-$Al_2O_3(1\bar{1}02)$

For sample dosing purposes D_2O was seeded in helium by bubbling He through a deuterated water reservoir. To minimize subsequent adsorption of D_2O on the tubes of the gas system before reaching the nozzle, all tubing was heated to 120°C. All measurements described below were performed using a nozzle temperature (i.e. T_{Nozzle}) of 860 K, which corresponds to a D_2O kinetic energy of ≈ 0.6 eV of per molecule. For dosing water on the sample we used following procedure:

(i) We start dosing with the MBS at $T_{Al_2O_3} = 400$ K and cool with a 10 K/min ramp to 130 K while dosing.

(ii) Align the VSF spectrometer on the large free OD signal from ice by overlapping the visible and infrared beams spatially and temporally (a precondition for the VSF measurement).

(iii) Anneal the surface with a ramp of 100 K/min to 185 K or higher to remove the great majority of all molecularly adsorbed water and return the sample to 135 K for VSF characterisation.

1.4 Technical Details of VSF Spectrometer

In our VSF spectrometer we employ a Legend Elite Duo amplifier system (Coherent) with a pulse energy of 8 mJ, a pulse length of 50 fs, a spectrum centered at 800 nm and a repetition rate of 1 KHz. 5mJ of this pulse energy is sent to a TOPAS (Coherent) to generate broadband IR laser pulses. Those pulses (bandwidth 190 - 230 cm^{-1} (FWHM)) have energies of 30 - 40 μJ. The VIS laser in the VSF interaction is generated by narrowing the remaining 800 nm pulse after the TOPAS in a homebuilt pulse shaper to obtain pulses of 25 μJ and a FWHM of ≈ 8 cm^{-1}. The incident angles in our setup were 75/70 degrees for Vis/IR. Our experimental configuration was such that both incident beams and the emitted VSF were co-planar and this plane was perpendicular to the plane of the surface. All spectrum shown were collected using polarization combination of *ppp* (VSF/Vis/IR) in which *p* indicates parallel to the plane of incidence. Polarization of all incident and detected fields was accomplished by using $\lambda/2$ wave plate, polarizer, $\lambda/2$ wave plate combinations. The emitted sum frequency field was dispersed using a grating (1800 g/mm) and detected employing an ICCD camera from Princeton Instruments.

1.5 VSF Data Analysis

Analysis of the VSF data was done by dividing the collected signal by its corresponding nonresonant signal (to account for the frequency dependence of the incident infrared energy) and then fitting the data using equations 1 and 2 and the Levenberg-Marquardt algorithm as implemented in the analysis program Igor Pro (Wavemetrics). Following prior workers we constrained this fit by taking the phase of the nonresonant contribution to be zero. We further assume that the phase of each resonance is independent of temperature. Treating the line width (Γ), center frequency ($\tilde{\nu}_q$) and amplitude ($|A_q|$) of each resonance as fit parameters leads to a description of the data in which both center frequency and line width are relatively constant as a function of temperature while amplitude varies greatly. Attempts to fit the data with initial guesses for amplitude that vary over several orders of magnitude and phases between 0 and 2π suggests that the resulting fit is relatively insensitive to these choices. Initial guesses for $\tilde{\nu}_q$ that vary by > 35 cm^{-1}

OD species	$\tilde{\nu}_q$ (cm^{-1})	Γ (cm^{-1})	$\lvert A_q \rvert$(a.u.)	$\phi_R(\pi)$
$OD_{ice,135K}$	2723	12	400	0.5
$OD_{mol,ads,185K}$	2732	26	33	0.1
$OD_{diss,ads,185K}$	2772	37	28	0.2

Table 1: Results from applying the line shape model in the using the procedure described above for an ice sample and a sample at 185 K.

from the tabulated results lead to non-physical local minima.

$$I_{\mathrm{VSF}} \propto \left|\chi^{(2)}_{\mathrm{eff}}\right|^2 \tag{1}$$

$$\chi^{(2)}_{\mathrm{eff}} \propto |A_{\mathrm{NR}}| \; e^{\mathrm{i}\phi_{\mathrm{NR}}} + \sum_q \frac{|A_q| e^{\mathrm{i}\phi_{\mathrm{R}}}}{\tilde{\nu}_{\mathrm{IR}} - \tilde{\nu}_q + i\Gamma_q} \tag{2}$$

2 Linking I_{VSF} and OD angle

By monitoring the intensity of the emitted VSF signal as a function of incident IR frequency, we recover a vibrational spectrum of all the OD containing moieties at the surface. This observed VSF spectral response is a function of the microscopic nonlinear susceptibility, the incident beam angles, refractive indices of both bulk phases and the interface and molecular orientation. The manner in which these physical aspects of the interfacial system relate has been well described in the literature [5–9], here we review the aspects of this theory relevant to understanding the VSF data reported in this study.

Taking the emitted sum frequency field to come from a polarization sheet at the α-Al_2O_3/vacuum interface and solving Maxwell's equations gives,

$$I_{\mathrm{VSF}}(\tilde{\nu}_{\mathrm{IR}}) = \frac{8\pi^3 \tilde{\nu}^2_{\mathrm{VSF}}}{c^3 cos^2 \beta_{\mathrm{VSF}}} \left|\chi^{(2)}_{\mathrm{eff}}\right|^2 I_{\mathrm{VIS}} I_{\mathrm{IR}}(\tilde{\nu}_{\mathrm{IR}}) \tag{3}$$

in which $I_{\mathrm{VSF}}(\tilde{\nu}_{\mathrm{IR}})$ is the intensity of the emitted sum frequency field (which is a function of the frequency of the incident infrared), $\tilde{\nu}_i$ is the frequency of the i^{th} field, c is the speed of light in vacuum, β_{VSF} is the angle of the wave vector of the reflected SF field with respect to the surface normal, I_{VIS} is the intensity of the visible field and $I_{\mathrm{IR}}(\tilde{\nu}_{\mathrm{IR}})$ is the intensity of the incident infrared, which is frequency dependent. With the exception of $\chi^{(2)}_{\mathrm{eff}}$ all of these parameters are either under the control of the experimentalist or are physical constants.

$\chi^{(2)}_{\rm eff}$, the macroscopic nonlinear susceptibility, contains all sample specific information. Because our surface has macroscopic $C_{\infty v}$ symmetry, 7 of the 27 elements of $\chi^{(2)}_{\rm eff}$ are nonzero and only 4 are independent. In a laboratory reference frame in which (x,y) is the plane of the surface and z the surface normal, these are $\chi^{(2)}_{zzz}$, $\chi^{(2)}_{xzx} = \chi^{(2)}_{yzy}$, $\chi^{(2)}_{xxz} = \chi^{(2)}_{yyz}$ and $\chi^{(2)}_{zxx} = \chi^{(2)}_{zyy}$. If we further assume that all beams propagate in the x-z plane and s indicates polarization perpendicular and p parallel to the x-z plane, we can write explicit expressions relating the experimentally controllable parameters, beam polarizations and angles, to the $\chi^{(2)}_{\rm eff}$. For $\chi^{(2)}_{\rm eff,ssp}$ and $\chi^{(2)}_{\rm eff,ppp}$ the relevant equations are,

$$\begin{aligned}
\chi^{(2)}_{\rm eff,ssp} &= L_{yy}(\tilde{\nu}_{\rm VSF})L_{yy}(\tilde{\nu}_{\rm VIS})L_{zz}(\tilde{\nu}_{\rm IR})\sin\beta_{\rm IR}\chi^{(2)}_{yyz} \qquad (4)\\
\chi^{(2)}_{\rm eff,ppp} &= -L_{xx}(\tilde{\nu}_{\rm VSF})L_{xx}(\tilde{\nu}_{\rm VIS})L_{zz}(\tilde{\nu}_{\rm IR})\cos\beta_{\rm VSF}\cos\beta_{\rm VIS}\sin\beta_{\rm IR}\chi^{(2)}_{xxz}\\
&\quad -L_{xx}(\tilde{\nu}_{\rm VSF})L_{zz}(\tilde{\nu}_{\rm VIS})L_{xx}(\tilde{\nu}_{\rm IR})\cos\beta_{\rm VSF}\sin\beta_{\rm VIS}\cos\beta_{\rm IR}\chi^{(2)}_{xzx}\\
&\quad +L_{zz}(\tilde{\nu}_{\rm VSF})L_{xx}(\tilde{\nu}_{\rm VIS})L_{xx}(\tilde{\nu}_{\rm IR})\sin\beta_{\rm VSF}\cos\beta_{\rm VIS}\cos\beta_{\rm IR}\chi^{(2)}_{zxx}\\
&\quad +L_{zz}(\tilde{\nu}_{\rm VSF})L_{zz}(\tilde{\nu}_{\rm VIS})L_{zz}(\tilde{\nu}_{\rm IR})\sin\beta_{\rm VSF}\sin\beta_{\rm VIS}\sin\beta_{\rm IR}\chi^{(2)}_{zzz}
\end{aligned}$$

in which $\sin\beta_k$ is the incident angle for the beam k and $L_{ij}(\tilde{\nu})$ are the Fresnel coefficients. These coefficients can be written,

$$L_{xx}(\tilde{\nu}) = \frac{2\cos\gamma_{\tilde{\nu}}}{\cos\gamma_{\tilde{\nu}} + n_{Al_2O_3}(\tilde{\nu})\cos\beta_{\tilde{\nu}}} \qquad (5)$$

$$L_{yy}(\tilde{\nu}) = \frac{2\cos\beta_{\tilde{\nu}}}{\cos\beta_{\tilde{\nu}} + n_{Al_2O_3}(\tilde{\nu})\cos\gamma_{\tilde{\nu}}} \qquad (6)$$

$$L_{zz}(\tilde{\nu}) = \frac{2n_{Al_2O_3}(\tilde{\nu})\cos\beta_{\tilde{\nu}}}{\cos\gamma_{\tilde{\nu}} + n_{Al_2O_3}(\tilde{\nu})\cos\beta_{\tilde{\nu}}}\left(\frac{1}{n'(\tilde{\nu})}\right) \qquad (7)$$

in which $\beta_{\tilde{\nu}}$

The macroscopic nonlinear susceptibility in the laboratory frame $\chi^{(2)}_{ijk}$ can be connected to the molecular hyperpolarizability $\alpha_{i'j'k'}$,

$$\chi^{(2)}_{ijk} = \frac{1}{2\epsilon_0}N_s\langle R_{ii'}R_{jj'}R_{kk'}\rangle\alpha_{i'j'k'} \qquad (8)$$

in which $\langle R_{ii'}R_{jj'}R_{kk'}\rangle$ is the ensemble averaged transformation matrix between molecular and laboratory coordinates in the *slow motion limit*: in which the angle of individual OD groups with respect to the surface normal (θ) does not change on the timescale of the inverse line width. It is unlikely that our system rigorously meets this condition but, as has been discussed in the previous literature in detail (see [9] and refs therein), for physically realistic motion of OD groups the effect on relative OD intensities with changing experimental geometry is likely to be small (note here that all measurements are performed at 135 K). Given this assumption, evaluating the $\langle R_{ii'}R_{jj'}R_{kk'}\rangle$ matrix for each of the relevant $\chi^{(2)}_{ijk}$ terms gives,

$$
\begin{aligned}
\chi^{(2)}_{yyz} &= \chi^{(2)}_{xxz} = \frac{1}{2\epsilon_0} N_s \alpha^{(2)}_{z'z'z'} \left[\left\langle sin^2\theta \; cos\theta \right\rangle (1-r) + 2r \left\langle cos\theta \right\rangle \right] \\
\chi^{(2)}_{xzx} &= \chi^{(2)}_{zxx} = \frac{1}{2\epsilon_0} N_s \alpha_{z'z'z'} \left(\langle \cos\theta \rangle - \langle \cos^3\theta \rangle \right) (1-r) \\
\chi^{(2)}_{zzz} &= \frac{1}{\epsilon_0} N_s \alpha_{z'z'z'} \left[r \langle \cos\theta \rangle + \langle \cos^3\theta \rangle (1-r) \right] \qquad (9)
\end{aligned}
$$

in which N_s is the number of molecules at the surface, $\alpha^{(2)}_{z'z'z'}$ is the hyperpolarizability along the molecular axis z', r is is the hyperpolarizability ratio ($r = \frac{\alpha_{y'y'z'}}{\alpha_{z'z'z'}}$) and θ is the angle with respect to the surface normal. To actually calculate the relationship between I_{VSF} and θ as presented in the text and below we have assumed that all non-hydrogen bonded OD have similar $\alpha_{z'z'z'}$ and r and used the values for these quantitates from our prior publication [10]. Note that, because we desire insight only into the *relative* change in $\mathrm{I_{VSF}}$ as a function of molecular orientation, knowledge of the surface density of OD groups is not required.

3 Computational Details

3.1 Additional Structural Parameters of Adsorbed D_2O

As discussed in the text we principally consider eight possible OD groups in this paper. Two of these are contained in an intact D_2O molecule adsorbed in the 1-2 configuration, two in an intact D_2O molecule adsorbed in the 1-4 configuration, two in a dissociatively adsorbed D_2O molecule in the 1-2 configuration and two in a dissociatively adsorbed D_2O molecule in the 1-4 configuration. In the manuscript the angle formed by each of these eight OD groups with the surface normal is tabulated. We here provide additional structural parameters.

Table 2: Structural parameters from the four structures illustrated in Figures 4 and 5 in the manuscript. Al-O_{D_2O} indicates the bond between a surface Al and the oxygen in an adsorbed D_2O. Al-O_{D_2O} angle is the angle of the Al-O_{D_2O} bond vector with respect to the surface normal.

Structures	1-4 molec	1-4 dissoc	1-2 molec	1-2 dissoc
Al-O_{D_2O} bond length [Å]	1.94	1.80	2.00	1.75
Al-O_{D_2O} angle [°]	35.5	37.1	13.1	22.2
OD_{ads} bond length [Å]	0.97	0.97	0.98	0.97
OD_{surf} bond length [Å]	1.54	1.03	2.03	0.98

References

[1] J. W. Elam, C. E. Nelson, M. A. Cameron, M. A. Tolbert, and S. M. George, "Adsorption of H_2O on a Single-Crystal α-Al_2O_3(0001) Surface," *J. Phys. Chem. B*, vol. 102, pp. 7008–7015, 1998.

[2] C. Niu, C. Shepherd, D. Martini, J. A. Kelber, D. R. Jennison, and A. Bogicevic, "Cu interactions with α-Al_2O_3(0001): Effects of Surface Hydroxyl Groups vs Dehydroxylation by Ar Ion Sputtering," *Surf. Sci.*, vol. 465, pp. 163–176, 2000.

[3] T. P. Trainor, P. J. Eng, G. E. Brown, I. K. Robinson, and M. D. Santis, "Crystal truncation rod diffraction study of the α-$Al_2O_3(1\bar{1}02)$ surface," *Surf. Sci.*, vol. 496, no. 3, pp. 238–250, 2002.

[4] M. Schildbach and A. Hamza, "Clean and water-covered sapphire $(1\bar{1}02)$ surfaces: structure and laser-induced desorption," *Surf. Sci.*, vol. 282, no. 3, pp. 306–322, 1993.

[5] P. Guyot-Sionnest, W. Chen, and Y. R. Shen, "General Considerations on Optical Second-Harmonic Generation from Surfaces and Interfaces," *Phys. Rev. B*, vol. 33, no. 12, pp. 8254–8263, 1986.

[6] X. D. Zhu, H. Suhr, and Y. R. Shen, "Surface Vibrational Spectroscopy by Infrared-Visible Sum Frequency Generation," *Phys. Rev. B*, vol. 35, no. 6, pp. 3047–3050, 1987.

[7] T. F. Heinz, "Second-Order Nonlinear Optical Effects at Surfaces and Interfaces," in *Nonlinear Surface Electromagnetic Phenomena* (H. E. Ponrath and G. I. Stegeman, eds.), pp. 353–416, Elsevier Science Publishers, 1991.

[8] C. D. Bain, P. B. Davies, T. H. Ong, R. N. Ward, and M. A. Brown, "Quantitative Analysis of Monolayer Composition by Sum-Frequency Vibrational Spectroscopy," *Langmuir*, vol. 7, no. 8, pp. 1563–1566, 1991.

[9] H.-F. Wang, W. Gan, R. Lu, Y. Rao, and B.-H. Wu, "Quantitative Spectral and Orientational Analysis in Surface Sum Frequency Generation Vibrational Spectroscopy (SFG-VS)," *Int. Rev. Phys. Chem.*, vol. 24, no. 2, pp. 191–256, 2005.

[10] Y. Tong, A. Vila Verde, and R. K. Campen, "The Free OD at the Air/D_2O Interface Is Structurally and Dynamically Heterogeneous," *J. Phys. Chem. B*, vol. 117, no. 39, pp. 11753–11764, 2013.